Cerebral Cortex, June 2016;26: 2612–2625

doi: 10.1093/cercor/bhv099
Advance Access Publication Date: 15 May 2015
Original Article

ORIGINAL ARTICLE

Thalamocortical Innervation Pattern in Mouse Auditory and Visual Cortex: Laminar and Cell-Type Specificity

Xu-ying Ji[1,2], Brian Zingg[2,5], Lukas Mesik[2,5], Zhongju Xiao[1], Li I. Zhang[2,4], and Huizhong W. Tao[2,3]

[1]Department of Physiology, School of Basic Medical Sciences, Southern Medical University, Guangzhou 510515, China, [2]Zilkha Neurogenetic Institute, [3]Department of Cell and Neurobiology, [4]Department of Biophysics and Physiology and [5]Neuroscience Graduate Program, Keck School of Medicine, University of Southern California, Los Angeles, CA 90089, USA

Address correspondence to Zhongju Xiao. Email: xiaozj@smu.edu.cn

Abstract

Despite many previous studies, the functional innervation pattern of thalamic axons and their target specificity remains to be investigated thoroughly. Here, in primary auditory cortical slices, we examined thalamic innervation patterns for excitatory and different types of inhibitory neurons across laminae, by optogenetically stimulating axons from the medial geniculate body. We found that excitatory cells and parvalbumin (PV)-expressing inhibitory neurons across layer 2/3 (L2/3) to L6 are directly innervated by thalamic projections, with the strongest innervation occurring in L4. The innervation of PV neurons is stronger than that of excitatory neurons in the same layer, with a relatively constant ratio between their innervation strengths across layers. For somatostatin and vasoactive intestinal peptide inhibitory neurons, essentially only L4 neurons were innervated by thalamic axons and the innervation was much weaker compared with excitatory and PV cells. In addition, more than half of inhibitory neurons in L1 were innervated, relatively strongly, by thalamic axons. Similar innervation patterns were also observed in the primary visual cortex. Thus, thalamic information can be processed independently and differentially by different cortical layers, in addition to the generally thought hierarchical processing starting from L4. This parallel processing is likely shaped by feedforward inhibition from PV neurons in each individual lamina, and may extend the computation power of sensory cortices.

Key words: cortical inhibitory neuron, laminar distribution, pyramidal cell, sensory cortex, thalamic innervation, thalamocortical projection, SOM neuron, VIP neuron

Introduction

In mammals, sensory information is relayed by the thalamus into the primary sensory cortex of the corresponding modality. In the cortex, it has been thought that information is processed in a serial, vertical manner across cortical laminae (Callaway 1998; Douglas and Martin 2004). L4 is the major thalamorecipient layer, and relays thalamic signals to supragranular layers (L2/3) before the signals are further transmitted to infragranular layers (L5/6). This hierarchical model has been supported by anatomical evidence that axons of L4 principal neurons primarily innervate L2/3 and that axons of L2/3 pyramidal neurons arborize extensively in L5/6 (Gilbert and Wiesel 1979; Feldmeyer 2012). However, examinations of anterogradely labeled thalamocortical axons indicate that they terminate in nearly all cortical layers (White 1978; Frost and Caviness 1980; Romanski and LeDoux 1993; Citas et al. 1999; Oberlaender et al. 2012; Smith et al. 2012). Indeed, in vitro and in vivo whole-cell recordings in the primary somatosensory ("barrel") and primary auditory cortices have demonstrated that neurons in supra- and infragranular layers can also receive direct thalamic inputs (Mitani et al. 1985; Yamamoto et al. 1990; Agmon and Connors 1992; Armstrong-James et al.

1992; Zhou et al. 2010; Viaene et al. 2011a; 2011b; Constantinople and Bruno 2013; Sun et al. 2013). These data suggest that the thalamic innervation of sensory cortical neurons could be extensive beyond L4.

Thalamic inputs to L4 neurons have been extensively studied in vitro (Agmon and Connors 1991, 1992; Porter et al. 2001;Cruikshank et al. 2002; Beierlein et al. 2003; Gabernet et al. 2005; Rose and Metherate 2005; Inoue and Imoto 2006; Sun et al. 2006; Barkat et al. 2011; Schiff and Reyes 2012) and in vivo (Ferster and Lindström 1983; Chung and Ferster 1998; Moore and Nelson 1998; Liu et al. 2007; Li, Ibrahim et al. 2013; Li, Li et al. 2013; Lien and Scanziani 2013). In those studies, excitatory and inhibitory neurons in this thalamorecipient layer were most often distinguished by their different firing patterns to current injections (e.g., Agmon and Connors 1992; Porter et al. 2001; Beierlein et al. 2003). Only recently, genetically identified inhibitory neurons are beginning to be examined in specific layers of the cortex (Tan et al. 2008; Cruikshank et al. 2010). In view of the limited results from those previous studies, a comprehensive characterization of the thalamic innervation of cortical neurons across laminae and of identified cells types is necessary for a deeper understanding of thalamocortical transformation.

Conventionally, thalamocortical responses were studied in thalamocortical slice preparations. The thalamus (or thalamocortical axon tracts) has been activated electrically, and the resulting cortical responses have been recorded with electrophysiological or optical techniques. A concern over electrical stimulation is that it may activate nontargeted neurons and axonal/dendritic processes near the stimulation electrodes. Recently, optogenetic techniques have been introduced in studies of long-range axonal projections (Petreanu et al. 2007, 2009; Cruikshank et al. 2010). By expressing channelrhodopsin-2 (ChR2), a light-sensitive cation channel (Nagel et al. 2003), mammalian neurons could be excited by blue light with high temporal precision (Boyden et al. 2005; Cardin et al. 2009; Gradinaru et al. 2009). More importantly, enough ChR2 could be expressed in the axons and terminals of those neurons that the terminal arbors themselves could be directly excited by light, triggering transmitter release without the need for illumination of parent somata (Petreanu et al. 2007). Therefore, with optogenetics, long-range axonal projections can be examined in a more specific manner. In this study, by expressing ChR2 in the thalamus in various cell-type-specific mouse lines, we examined thalamocortical innervation patterns of different cortical cell classes across laminae.

Materials and Methods

Animal Preparation

All experiment procedures were approved by the Animal Care and Use Committee at the University of Southern California. Both male and female adult (P50–P70) mice were used for experiments. Animals were housed in a vivarium with a 12 h light/dark cycle. Transgenic mouse lines used include PV-Cre, SOM-Cre, VIP-Cre, GAD2-Cre (The Jackson Laboratory), and GAD1-GFP (from Dr Yuchio Yanagawa, Brain Science Institute, RIKEN, Japan). To visualize inhibitory neurons of desired types, PV-Cre, SOM-Cre, VIP-Cre, and GAD2-Cre mice (Taniguchi et al. 2011) were crossed with the Ai14 (Cre-dependent tdTomato) reporter line (Madisen et al. 2012).

Viral Injection

AAV2/9.EF1α.DIO.hChR2(H134R)-EYFP.WPRE.hGH (Addegene 20298) virus was injected to the left medial geniculate body (MGB) (3.2 mm caudal to Bregma and 2 mm lateral to midline at the depth of 3 mm) or to the left dorsal lateral geniculate nucleus (dLGN) (2.3 mm caudal to Bregma and 2.2 mm lateral to midline at the depth of 2.75 mm) of adult Cre mice (PV-Cre, SOM-Cre,VIP-Cre or GAD2-Cre;Ai14) or GAD1-GFP pigmented mice, as described previously (Li, Li et al. 2013; Li, Xiong et al. 2015). The virus was delivered using a beveled glass micropipette (tip diameter: ~30–40 μm) attached to a microsyringe pump (World Precision Instruments). For each injection, 100 nl of the viral solution was injected at a rate of 20 nl/min. Right after each injection, the pipette was allowed to rest for 4 min before withdrawal. The scalp was then sutured. Following the surgery, 0.1 mg/kg buprenorphine was injected subcutaneously before returning the animals back to their home cages. Three to 4 weeks after the injections, the mice were used for slice recording.

Slice Preparation

Thalamocortical slices were prepared following a previous study (Cruikshank et al. 2002). Viral injected mice were anesthetized with urethane. After decapitation, the brain was rapidly removed into an ice-cold oxygenated dissection buffer (60 mM NaCl, 3 mM KCl, 1.25 mM NaH_2PO_4, 25 mM $NaHCO_3$, 115 mM sucrose, 10 mM glucose, 7 mM $MgCl_2$, 0.5 mM $CaCl_2$; bubbled with 95% O_2 and 5% CO_2; pH = 7.4). Thalamocortical slices of 350 μm thickness were cut from the infected brain hemisphere by a vibrating microtome (Leica VT1000s). After being incubated in a warmed (at 34°C) artificial cerebral spinal fluid (ACSF; 126 mM NaCl, 2.5 mM KCl, 1.25 mM NaH_2PO_4, 26 mM $NaHCO_3$, 1 mM $MgCl_2$, 2 mM $CaCl_2$, 0.5 mM ascorbic acid, 2 mM sodium pyrurate, and 10 mM glucose, bubbled with 95% O_2 and 5% CO_2) for >30 min, the slice was transferred to the recording chamber at room temperature.

Electrophysiological Recording

Recording was made under an upright fluorescence microscope (Olympus BX51WI) equipped with an infrared light source. Slices were examined under a 4× objective before recording to determine whether ChR2-EYFP was expressed in the appropriate site (within the MGB or dLGN). In slices with good expression sites, whole-cell voltage-clamp recordings were selectively performed on fluorescence-labeled inhibitory neurons in PV-Cre, SOM-Cre, VIP-Cre or GAD2-Cre;Ai14 slices or non-fluorescent excitatory cells in GAD1-GFP slices under epifluorescence imaging. The extracellular solution contained: 126 mM NaCl, 2.5 mM KCl, 1.25 mM NaH_2PO_4, 26 mM $NaHCO_3$, 1 mM $MgCl_2$, 2 mM $CaCl_2$, 0.5 mM ascorbic acid, 2 mM sodium pyrurate,10 mM glucose, and bubbled with 95% O_2 and 5% CO_2. For examining thalamocortical responses only, recordings were made with TTX (tetrodotoxin; a sodium channel blocker, 1 μM) and 4-aminopyridine (a potassium channel blocker, 1 mM) present in the external solution so that only monosynaptic responses could be observed. For voltage-clamp recordings, glass pipette (4–7 MΩ impedance) was filled with a cesium-based internal solution (125 mM Cs-gluconate, 5 mM TEA-Cl, 4 mM MgATP, 0.3 mM GTP, 10 mM phosphocreatine, 10 mM HEPES, 1 mM EGTA, 2 mM CsCl, 1% biocytin, pH = 7.2). For current-clamp recordings, a potassium-based internal solution (125 mM K^+-gluconate, 10 mM HEPES, 10 mM EGTA, 4 mM Mg-ATP, 0.3 mM GTP, 2 mM KCl, 0.1 mM $CaCl_2$, 8 mM phosphocreatine sodium, pH = 7.2) was used. The pipette and whole-cell capacitances were completely compensated and the initial series resistance was compensated for 50% at 100 μS lag. Excitatory and inhibitory synaptic currents were recorded by clamping the cell's membrane potential at –70 and 0 mV respectively. Recordings were made with an Axopatch 200B

amplifier (Molecular Devices). Signals were filtered at 2 kHz and sampled at 10 kHz. In each slice, multiple neurons were recorded. The cortical depth of each recorded cell was based on the vertical distance of the cell body from the pial surface of the cortex, which was set as 0 μm. The distance was measured with a micromanipulator coupled with a digital reader (SD Instrument DR1000). Morphologies of some recorded cells were reconstructed through previously described histological procedures of biocytin labeling (Wu et al. 2008; Zhou et al. 2010).

Photostimulation

ChR2 was activated by blue light pulses from a mercury Arc lamp gated by an electronic shutter (Li, Ji et al. 2014). The excitation light was passed through a blue light filter and the objective. A calibrated aperture placed at the conjugated plane of the slice was used to control the size of the illumination area. The aperture was adjusted so that the entire A1 or V1 area was illuminated. The power of light stimulation was 3 mW measured at the focal plane. Brief light pulses (3 ms) were applied individually (0.033 Hz). For each condition, 10–30 trials were tested and responses were averaged.

Data Analysis

Peak amplitude was measured for each averaged response trace within 100 ms window after the onset of light stimulation. Response was only considered as evoked if the peak amplitude exceeded the average baseline level by 2 standard deviations (SDs) of baseline fluctuations. For each slice, peak response amplitudes of multiple (at least 3) excitatory neurons recorded in L4 were averaged. Such average values from multiple slices were further averaged to obtain a global average amplitude of L4 excitatory neuron responses. The experimentally observed amplitude of each cell was then scaled based on the ratio between the average L4 excitatory neuron response amplitude in the parent slice and the global average amplitude of L4 excitatory cell responses, as to obtain an adjusted amplitude. To calculate the ratio between strengths of thalamocortical inputs to excitatory versus inhibitory neurons, we used a bootstrap sampling method. In the data pool, each excitatory neuron response (in terms of adjusted amplitude) was randomly paired with an inhibitory neuron response in the same layer to calculate a "To E/To I ratio". Bootstrap sampling was performed for 1000 times for each cortical layer, and a mean value (and standard deviation) was obtained.

Retrograde Tracer Injection and Imaging

For retrograde labeling, 80 nl of fluorescently conjugated Cholera Toxin subunit B (CTb 488, 0.25%; Invitrogen) was injected into the A1 (4.5 mm, lateral to midline; −3.1 mm posterior to bregma; 0.5 mm down from pia) or A2/VAF (4.5 mm, lateral to midline; −3.0 mm posterior to bregma; 2 mm down from pia) through a pulled glass micropipette using a previously reported pressure injection method (Zingg et al. 2014). After 5–7 days, the animal was deeply anesthetized and transcardially perfused with 4% paraformaldehyde. Brain tissue was sliced into 150 μm sections using a vibratome and sections were mounted onto glass slides and imaged under a confocal microscope (Olympus).

The fluorescence intensity of thalamic projections to A1 was measured in Photoshop. To determine the range of intensity values across the vertical depth of the cortex, average fluorescence intensity was measured for 50 × 50 μm regions of interest, moving consecutively from the pial surface to the white matter.

Results

Thalamocortical Projections in the A1

To examine thalamocortical projections in the auditory cortex, we expressed ChR2 in thalamic axons by injecting an adeno-associated viral vector encoding ChR2 fused with EYFP into the MGB of adult mice (see Materials and Methods). Three to 4 weeks after the injection, strong expression of ChR2-EYFP were found in the MGB (Fig. 1A). In the auditory cortical area, fluorescence-labeled axons were most densely distributed in the primary auditory cortex (A1) (Fig. 1A). Examination of the laminar distribution of fluorescence in the A1 revealed that thalamic axons were distributed in all layers, with the strongest fluorescence in L4 (Fig. 1B). This is consistent with the notion that thalamocortical axons most strongly innervate L4 and deep L3 (Romanski and LeDoux 1993; Huang and Winer 2000; Winer et al. 2005; Llano and Sherman 2008; Smith et al. 2012). Imaging with lower levels of exposure revealed that retrograde labeling of deep layer neurons in the auditory cortex was extremely rare under our experimental conditions (Fig. 1C).

To examine the laminar pattern of functional innervation by thalamocortical projections, in brain slice preparations, we performed whole-cell voltage-clamp recordings from A1 neurons across layers, while optically stimulated thalamic axons by shining blue light on the entire auditory cortical area (see Materials and Methods). We first examined excitatory pyramidal neurons. By crossing a GAD2-Cre driver mouse line with a Cre-dependent tdTomato reporter line, Ai14 (Madisen et al. 2012), we could label all inhibitory neurons with red fluorescence, and selectively recorded from non-fluorescent neurons which were then excitatory (Fig. 1D). We recorded excitatory and inhibitory synaptic currents in response to stimulation of thalamic axons, by clamping the cell's membrane potential at −70 and 0 mV respectively. As shown in Figure 1E, a 3-ms pulse of blue light elicited an excitatory current and a nearly concurrent inhibitory current in the recorded neuron when the slice was bathed in the normal external solution. When TTX (1 μM) and 4-AP (1 mM) were perfused in, the inhibitory current disappeared and the excitatory current was reduced in amplitude (Fig. 1E, right panel), indicating that TTX plus 4-AP was effective in blocking disynaptic and polysynaptic responses, leaving only monosynaptic responses present (Petreanu et al. 2009; Cruikshank et al. 2010). Post hoc reconstruction of morphologies of some recorded cells confirmed that they were pyramidal excitatory neurons (Fig. 1F, left panel). These neurons exhibited low-frequency, adapting spikes in response to current injections, as examined in current-clamp recordings with a K-gluconate based internal solution (Fig. 1F, right panel).

To examine direct thalamic inputs, we then recorded monosynaptic excitatory responses with TTX and 4-AP always present in the external solution. In each slice, we sequentially recorded from multiple excitatory neurons across all layers, so that the evoked thalamocortical responses could be compared. Figure 1G shows 3 example slices where sample recorded cells located in L2/3 to L6 were compared. In each of these slices, we observed that excitatory neurons across all the layers were directly innervated by thalamocortical axons, as demonstrated by the presence of monosynaptic excitatory postsynaptic currents (EPSCs). EPSCs in L4 cells were apparently larger than those in other layers.

Laminar Pattern of Thalamocortical Innervation of Excitatory Neurons in the A1

Since there were variations in the level of ChR2 expression, for comparing the amplitudes of recorded thalamocortical responses

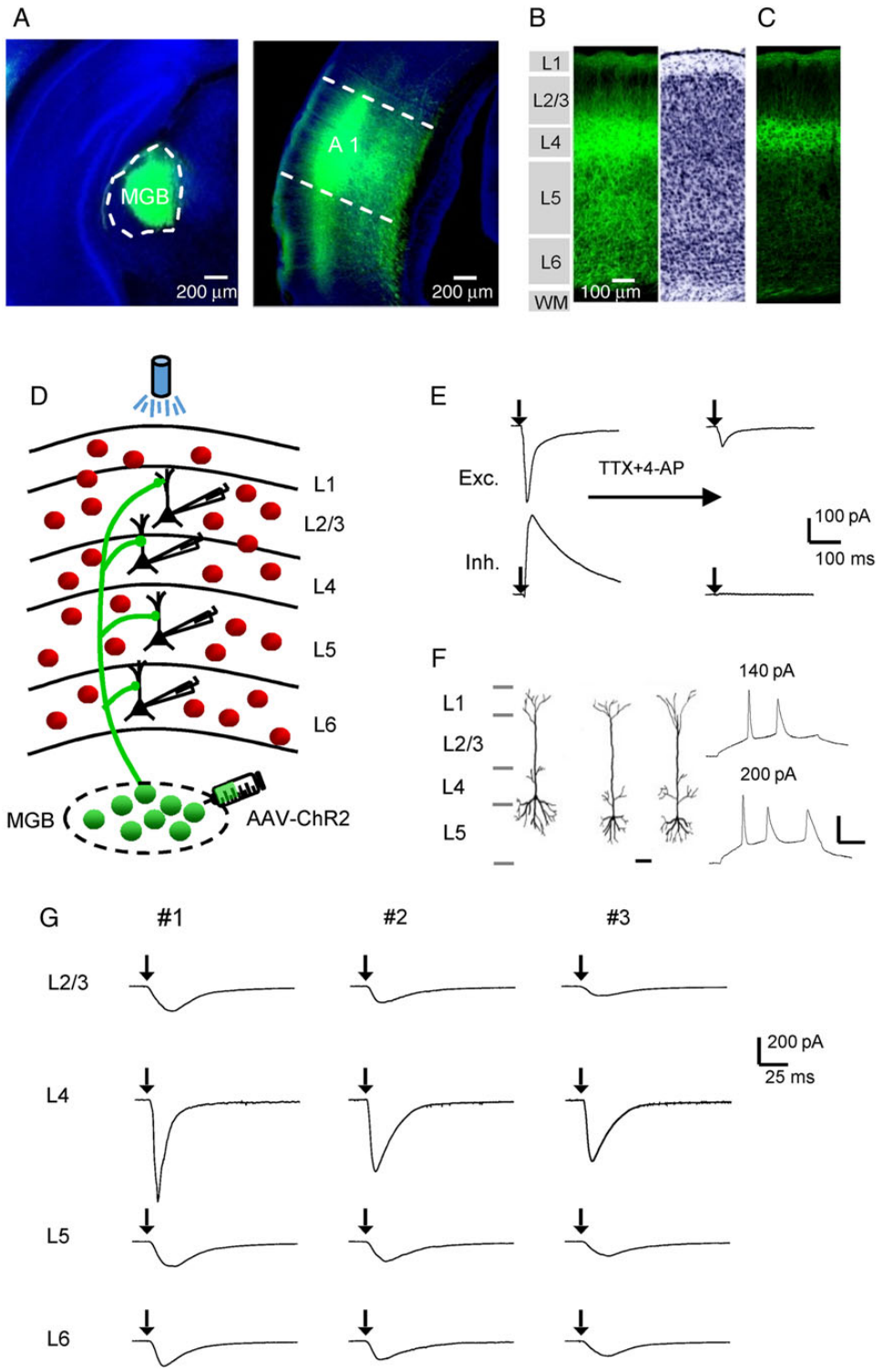

Figure 1. Laminar distribution of thalamocortical axons and functional examination of thalamocortical innervation. (*A*) Left, fluorescence image of the AAV-ChR2-EYFP injection site. The MGB is outlined. Blue, fluorescent nissl staining. Right, image of fluorescent axons in the auditory cortical area. A1 is outlined. The injection was performed on a P35 mouse and images were obtained at P56. (*B*) Laminar distribution of thalamocortical axons in the A1, with cytoarchitecturally defined cortical layers shown (left). Right, inverted image of fluorescent nissl staining. (*C*) Image of thalamocortical axons with a lower exposure level. Note that fluorescent cell bodies are absent in deep layers. Scale is the same as in (*B*). (*D*) Schematic graph showing laminar specific recordings from pyramidal neurons (black) in slices from GAD2-Cre;Ai14 mice, where inhibitory neurons are labeled by red fluorescence. Blue light was applied onto the entire auditory cortical area to stimulate thalamic axons expressing ChR2. (*E*) Excitatory (top) and inhibitory (bottom) postsynaptic currents (EPSC and IPSC respectively) of an example pyramidal neuron evoked by a 3-ms pulse of blue light (with onset marked by the arrow), recorded in the normal external solution (left) and after perfusing in TTX and 4-AP (right). (*F*) Left, reconstructed morphologies of 3 recorded cells, which confirmed that they were pyramidal cells. Scale: 50 µm. Right, membrane potential/spike responses of a pyramidal cell to current injections at 2 different levels. Scale: 20 mV and 50 ms. (*G*) Optically evoked monosynaptic EPSCs (averaged) of sample pyramidal neurons recorded in different layers of the same slice (vertically arranged). Three example slices (#1–#3) are shown. Black arrow marks the onset of photostimulation.

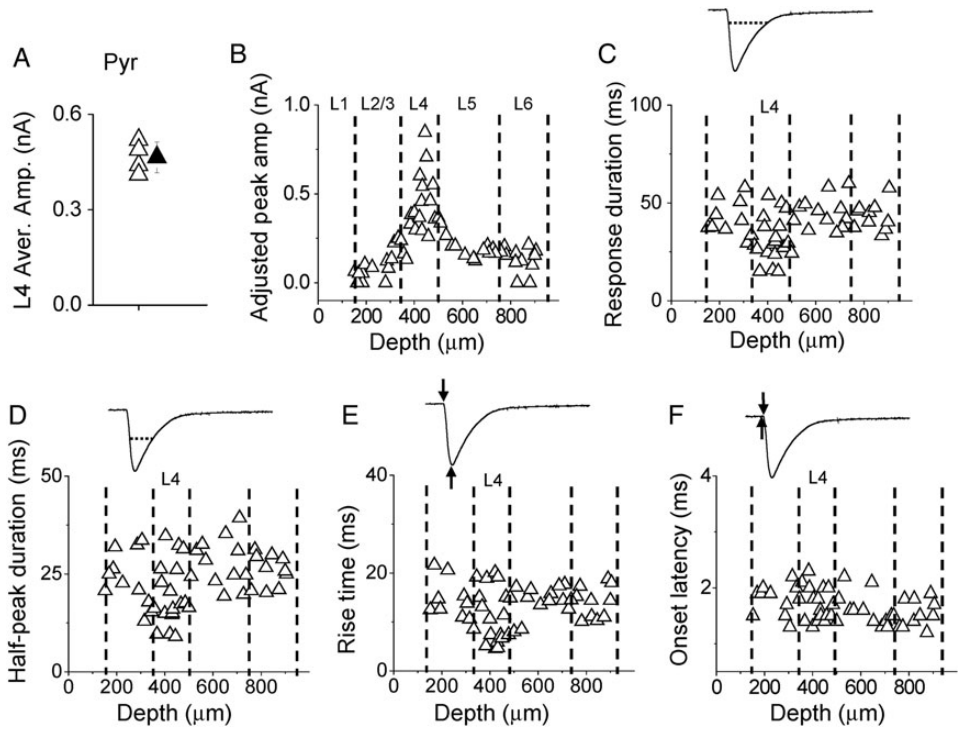

Figure 2. Laminar pattern of thalamocortical responses in A1 pyramidal neurons. (*A*) Average amplitudes of thalamocortical responses in L4 pyramidal neurons in 4 slices (open triangle) and their mean value (solid triangle, bar = SD). This global mean value could be used as a reference to calculate the adjusted amplitude for each recorded cell. (*B*) Distribution of adjusted peak amplitudes along cortical depth. Each data point represents one cell ($n = 56$ pyramidal cells from 4 slices). Recordings were made in the presence of TTX and 4-AP. Dotted lines indicate estimated boundaries between layers. (*C*) Distribution of response durations along cortical depth. Top inset, an example response trace showing that the duration was measured at the level of 10% of peak amplitude (marked by the dotted line). (*D*) Distribution of half-peak durations. Top inset, the dotted line shows that the duration was measured at the level of 50% of peak amplitude. (*E*) Distribution of response rise times. Top inset, the first arrow indicates the onset of the thalamocortical response, and the second arrow indicates the peak response. The interval between the 2 arrows defines the rise time. (*F*) Distribution of response onset latencies. Top inset, the first arrow indicates the onset of photostimulation, and the second arrow indicates the time when the response amplitude exceeds the average baseline by 2 SDs. The interval between the 2 arrows defines the onset latency.

among slices, we obtained a global average L4 response amplitude from the average L4 excitatory neuron responses in all slices (Fig. 2*A*), and scaled the response amplitude of each cell according to the ratio between the average L4 response amplitude in the parent slice and the global average amplitude (see Materials and Methods). This method was adapted from a previous study (Pfeffer et al. 2013). As shown in Figure 2*B*, in our recorded excitatory neuron population, thalamocortical responses appeared to be strongest in L4 (adjusted peak amplitude: 418 ± 180 pA in L4; 129 ± 75 pA in L2/3; 195 ± 58 pA in L5; 132 ± 70 pA in L6; mean ± SD; $F = 18.573$, $P = 0.000$, one-way ANOVA; $P < 0.001$ between L4 and L2/3, $P < 0.001$ between L4 and L5, $P < 0.001$ between L4 and L6, post hoc LSD test). Besides the peak amplitude, L4 responses also differed from other layers in terms of temporal response profile. Temporal duration of the thalamocortical response, as measured at the level of 10% of peak amplitude, was shortest in L4 [31.3 ± 11.6 ms in L4; 41.0 ± 9.7 ms in L2/3; 45.1 ± 8.0 ms in L5; 43.1 ± 7.1 ms in L6; $F = 6.137$, $P = 0.001$, analysis of variance (ANOVA) test; $P < 0.05$ between L4 and L2/3, $P < 0.001$ between L4 and L5, $P < 0.01$ between L4 and L6, post hoc test] (Fig. 2*C*). The half-peak duration of the thalamocortical response was also shortest in L4 (19.5 ± 7.9 ms in L4; 23.6 ± 7.0 ms in L2/3; 27.8 ± 6.2 ms in L5; 25.9 ± 4.1 ms in L6; $F = 4.229$, $P = 0.01$, ANOVA test; $P < 0.05$ between L4 and L2/3, $P < 0.01$ between L4 and L5, $P < 0.05$ between L4 and L6, post hoc test) (Fig. 2*D*). The response rise time, defined as the interval between the onset and peak of synaptic current, was shortest in L4 (10.9 ± 5.3 ms in L4; 14.6 ± 4.3 ms in L2/3; 14.8 ± 2.5 ms in L5; 14.1 ± 3.3 ms in L6; $F = 2.995$, $P = 0.04$, ANOVA test; $P < 0.05$ between L4 and L2/3; $P < 0.05$ between L4 and L5; $P < 0.05$ between L4 and L6, post hoc test) (Fig. 2*E*). These data on response dynamics imply that the thalamocortical synapses made on L4 pyramidal neurons are probably distributed on dendrites proximal to the soma (also see Richardson et al. 2009), while those on pyramidal cells in other layers may spread to dendritic regions relatively more distal. The response onset latencies were all >1.0 ms (Fig. 2*F*), longer than those for currents directly induced by ChR2 activation (< 0.2 ms, e.g., see Cruikshank et al. 2010). The onset latencies did not differ between layers (Fig. 2*F*), consistent with the notion that the evoked currents are all monosynaptic responses arising from activation of thalamic axon terminals.

Laminar Patterns of Thalamocortical Innervation of A1 Inhibitory Neurons

We next examined the thalamocortical innervation of different types of cortical inhibitory neurons, by injecting the AAV-ChR2 into the MGB of inhibitory cell-type-specific Cre driver lines crossed with Ai14. PV-Cre, SOM-Cre, and VIP-Cre lines (Taniguchi et al. 2011) were used, which together covered the great majority of inhibitory neurons (Rudy et al. 2011). As shown by the images of fluorescence-labeled cells, parvalbumin (PV) neurons were widely distributed throughout L2/3 to L6, but were absent in L1 (Fig. 3*A*). Somatostatin (SOM) neurons were also observed throughout L2/3 to L6, and were relatively more densely distributed in deep layers (Fig. 3*B*). In addition, since a subset of SOM neurons are Martinotti cells that project their axons into L1 (Markram et al. 2004; Wang

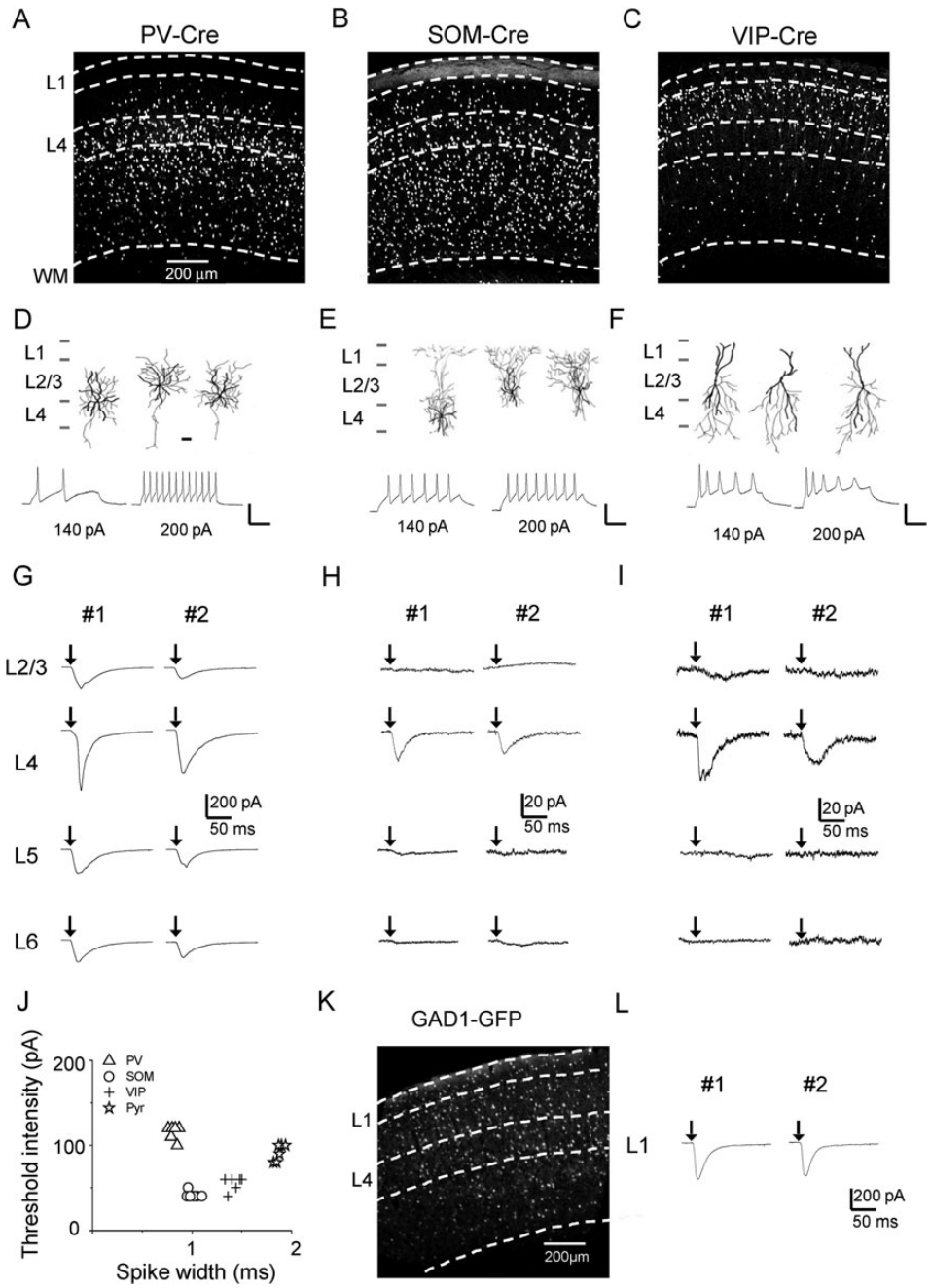

Figure 3. Thalamocortical innervation of A1 inhibitory neurons. (*A*) Fluorescence image of labeled PV neurons in the A1 of a PV-Cre;Ai14 mouse. (*B*) Fluorescence image of an A1 slice from a SOM-Cre;Ai14 mouse. (*C*) Image of an A1 slice from a VIP-Cre;Ai14 mouse. (*D*) Top, reconstructed morphologies (dark for dendrites, gray for axons) of 3 recorded PV neurons. Scale: 50 µm. Bottom, sample membrane potential/spike responses of a PV cell to current injections at 2 different levels. Scale: 50 pA and 50 ms. (*E*) Morphology and intrinsic spiking property for SOM neurons. (*F*) Morphology and intrinsic spiking property for VIP neurons. (*G*) Monosynaptic EPSCs recorded in sample PV cells in different layers of the same slice. Two example slices are shown. (*H*) EPSCs of example SOM neurons. (*I*) EPSCs of example VIP neurons. (*J*) Plot of threshold intensity of current injections that produce spikes vs. spike width for 4 types of neuron. Spike width was measured at the half-peak level above the spike threshold. (*K*) Fluorescence image of an A1 slice from a GAD1-GFP mouse. (*L*) EPSCs of example L1 inhibitory neurons recorded in 2 slices.

et al. 2004; Tan et al. 2008), L1 was also diffusely labeled by fluorescence in the SOM-Cre; Ai14 animal (Fig. 3*B*). Vasoactive intestinal peptide (VIP) neurons were mainly distributed in L2/3 and L4, but there were also scattered VIP neurons in deep layers and a very small number of VIP neurons in L1, in particular the lower part of L1 (Fig. 3*C*). We reconstructed morphologies for some recorded inhibitory cells. The results showed that PV cells had basket-cell morphologies (Fig. 3*D*, upper panel), SOM neurons mostly exhibited Martinotti-cell morphologies with axons ramifying in L1 (Fig. 3*E*, upper panel), and VIP neurons had bipolar morphologies (Fig. 3*F*, upper panel), all consistent with the known morphologies for these cell types (Markram et al. 2004). Current-clamp recordings using the K^+-based internal solution also revealed intrinsic spiking properties consistent with the cells' genetic identities: PV cells exhibited high-frequency, non-adapting fast spikes in response to positive current injections (Fig. 3*D*, lower

panel); SOM and VIP neurons had lower thresholds for spiking than PV and pyramidal cells and their spike widths were between those of PV and pyramidal cells (Fig. 3*E*, *F*, lower panel, and Fig. 3*J*). Using these cell-type-specific Cre lines with extremely low Cre leakage (Taniguchi et al. 2011), we could then selectively record from desired inhibitory cell types, and examined their thalamic inputs by optically stimulating thalamocortical axons.

As shown by example recording traces, PV neurons in L4 appeared to receive stronger excitation from thalamocortical axons as compared with other layers (Fig. 3*G*). SOM neurons in L4 received some thalamocortical innervation, but in other layers this inhibitory cell type received little innervation (Fig. 3*H*). Similar to SOM neurons, VIP neurons which received thalamocortical innervation were almost exclusively located in L4 (Fig. 3*I*). In L1, all neurons are inhibitory (Rudy et al. 2011). Since L1 neurons do not or rarely express PV, SOM, or VIP markers (Rudy et al. 2011), we used a GAD1-GFP transgenic line where all inhibitory neurons are labeled by GFP (Tamamaki et al. 2003) (Fig. 3*K*). Recordings from GFP-positive neurons in L1 showed that these inhibitory neurons also received thalamocortical innervation (Fig. 3*L*).

For comparing the strengths of thalamocortical innervation between different cell types as well as between different layers, we calculated an adjusted response amplitude for each recorded inhibitory cell, in a similar manner as for excitatory cell responses (see Materials and Methods). For PV neurons, we observed a similar laminar pattern of innervation strengths as pyramidal cells. While the great majority of PV neurons throughout L2/3 to L6 received direct thalamic inputs, the strongest innervation occurred in L4 (adjusted peak amplitude: 962 ± 341 pA in L4; 269 ± 168 pA in L2/3; 426 ± 130 pA in L5; 426 ± 50 pA in L6; $F = 25.479$, $P = 0.000$, ANOVA test; $P < 0.001$ between L4 and L2/3, $P < 0.001$ between L4 and L5, $P < 0.001$ between L4 and L6, post hoc test) (Fig. 4*A*). Interestingly, the laminar distribution of strengths of thalamocortical innervation for both PV and pyramidal neurons showed a good correspondence to the laminar distribution of fluorescence intensity of thalamocortical axon fibers (Fig. 4*J*, solid line, Pearson's correlation coefficient = 0.86 for PV and 0.83 for pyramidal), suggesting that the density of thalamocortical axons might primarily determine the strength of thalamocortical innervation of a given lamina. Different from pyramidal cells, the parameters for temporal profile of the thalamocortical responses in PV neurons did not show a distinction between different layers (Fig. 4*B*–*D*), suggesting that unlike pyramidal cells, the subcellular distribution of thalamocortical synapses on PV neurons may not have a lamina-specific pattern. Furthermore, the synaptic strength of thalamocortical innervation of PV neurons was in general stronger than that of pyramidal cells in the same layer (Fig. 4*J*,*K*).

Compared with PV and pyramidal cells, the thalamic innervation of SOM and VIP neurons was much weaker. In all layers except L4, these 2 types of inhibitory neuron essentially did not receive thalamocortical innervation (Fig. 4*E*,*F*). Even in L4, only less than half of the SOM and VIP population exhibited thalamocortical responses (Fig. 4*E*,*F*,*L*), while all PV and pyramidal neurons in this layer received direct thalamic inputs (Fig. 4*L*). In addition, for those SOM and VIP neurons that did receive thalamocortical innervation, the synaptic strength was much lower as compared with PV and pyramidal cells (adjusted peak amplitude: 20 ± 7 pA for SOM; 24 ± 11 pA for VIP; 962 ± 341 pA for PV; 418 ± 180 pA for pyramidal; $F = 35.05$, $P = 0.000$, ANOVA test; $P < 0.001$ between L4 SOM and L4 pyramidal, $P < 0.001$ between L4 SOM and L4 PV, $P < 0.001$ between L4 VIP and L4 pyramidal, $P < 0.001$ between L4 VIP and L4 PV, post hoc test). Therefore, most of SOM and VIP neurons appeared to avoid thalamocortical innervation. The response onset latencies for PV, SOM, and VIP neurons were as short as those for pyramidal cells ($F = 0.133$, $P = 0.94$, ANOVA test) (Fig. 4*G*–*I*), as expected for monosynaptic responses.

Finally, more than half of L1 inhibitory neurons received direct thalamic inputs (Fig. 4*J*,*L*). The thalamic inputs to L1 neurons were as strong as those to pyramidal cells in L4 (adjusted peak amplitude: 425 ± 129 pA for L1; 418 ± 180 pA for pyramidal; $P = 0.67$, *t*-test). Notably, L1 neurons which did not receive thalamocortical innervation were all located in the lower part of L1 (100–150 µm below the pia). This raises an interesting possibility that the upper and lower part of L1 may be functionally different to some extent.

Thalamocortical Innervation Patterns in the V1

To understand whether the laminar patterns of thalamocortical innervation observed in the A1 were common among different sensory modalities, we performed similar experiments in the primary visual cortex (V1). The AAV-ChR2 was injected into the dorsal lateral geniculate nucleus (dLGN) (Fig. 5*A*, top panel), the part of the thalamus that projects into V1. Weeks later whole-cell recordings were made in the V1 ipsilateral to the injected dLGN. Similar to what had been observed in the A1, in the V1, thalamic axons were most densely distributed in L4 and lower L2/3, but scattered axons were also observed in deep layers and L1 (Fig. 5*A*, bottom left panel). Retrograde labeling of deep layer neurons was not observed (Fig. 5*A*, bottom right panel). For both pyramidal and PV neurons, cells throughout L2/3 to L6 were widely innervated by thalamic axons, with the strongest innervation occurring in L4 (Fig. 5*B*,*C*). PV neurons exhibited a similar laminar profile of synaptic amplitude as pyramidal neurons, except that their thalamocortical responses were in general stronger than pyramidal cells (Fig. 5*E*). PV and pyramidal neurons in general exhibited a high probability of being innervated by thalamic axons (Fig. 5*F*). For SOM and VIP neurons, only those in L4 were observed to be directly innervated by thalamic axons, and only about one-third of the L4 population were innervated (Fig. 5*D*,*F*). The innervation was noticeably weak, with an amplitude only tenths of that for PV and pyramidal cells (Fig. 5*D*,*E*). As for L1 neurons, more than half of them were directly innervated by thalamic axons (Fig. 5*D*,*F*). Similar as observed in the A1, L1 neurons which were not innervated were all located in the lower part of L1 (Fig. 5*D*). Finally, the onset latencies for the evoked responses were similar across different cell groups, similar as in the A1 (Fig. 5*G*). Average response parameters are summarized for different cell groups in the A1 and V1 (see Table 1). Together, the thalamocortical innervation patterns in the V1 are in general consistent with those observed in the A1.

Distribution of Thalamic Neurons Innervating Auditory Cortical Areas

Our post hoc examination of infected brains revealed that in most cases AAV infection covered multiple divisions of the MGB (see Fig. 1*A*), raising the possibility that the recorded responses may have multiple thalamic input sources. To understand which thalamic area may provide the major input to the recorded cells in the A1, we carried out retrograde labeling experiments by injecting a standard retrograde tracer, CTb, into the A1 or VAF/A2 region (see Materials and Methods). We found that the thalamic inputs to A1 were primarily from the MGBv, and that the inputs to A2 were almost exclusively from thalamic nuclei surrounding the MGBv (Fig. 6*A*). Therefore, the first order thalamic nucleus (i.e., MGBv) provides the major input to the cells recorded in this study.

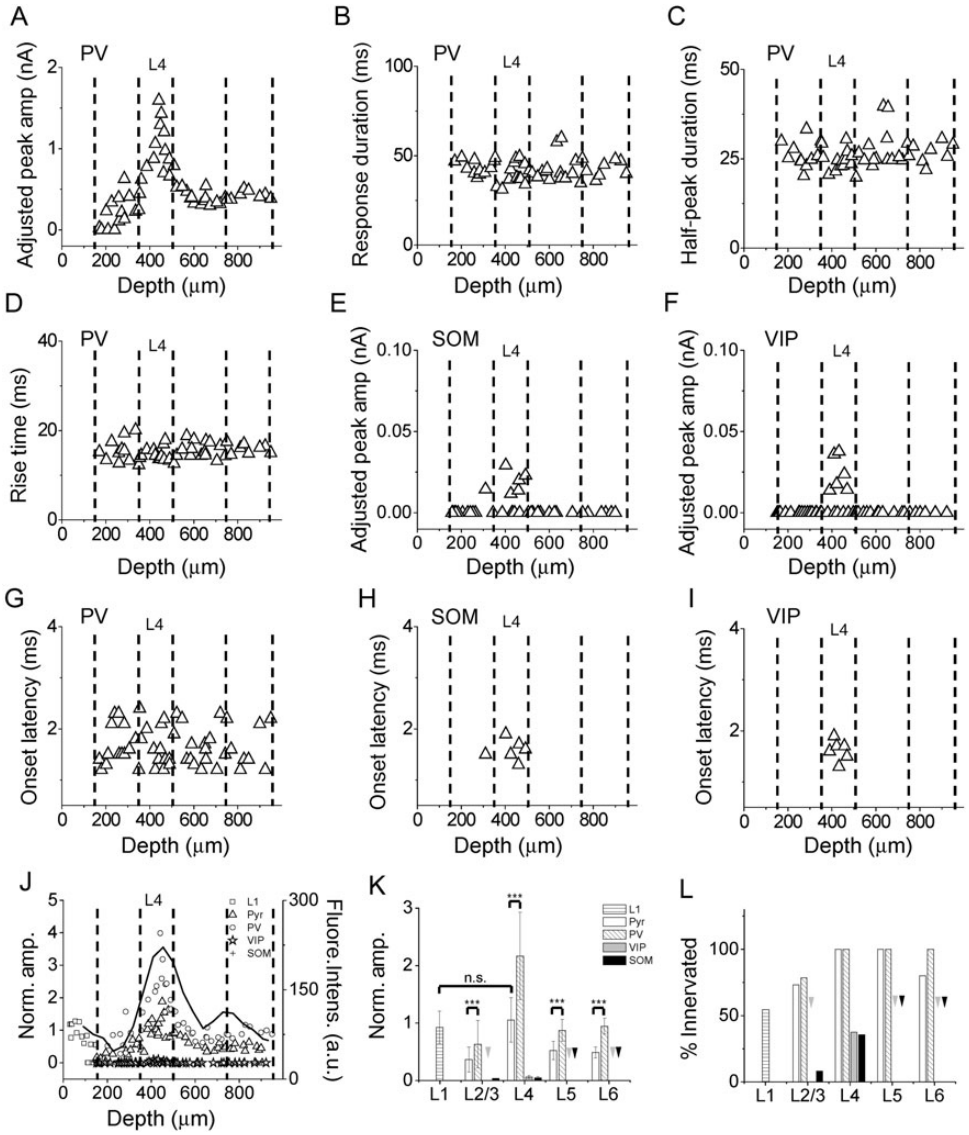

Figure 4. Laminar patterns of thalamocortical responses in A1 inhibitory neurons. (*A*) Distribution of adjusted peak amplitudes of thalamocortical responses recorded in PV neurons along cortical depth. Each data point represents one cell. (*B*) Distribution of response durations of thalamocortical responses in PV neurons. $F = 0.499$, $P = 0.685$, ANOVA test. (*C*) Distribution of half-peak durations for PV neurons. $F = 0.877$, $P = 0.461$, ANOVA test. (*D*) Distribution of response rise times for PV neurons. $F = 0.851$, $P = 0.474$, ANOVA test. (*E*) Distribution of adjusted peak amplitudes for SOM neurons. (*F*) Distribution of adjusted peak amplitudes for VIP neurons. (*G*) Distribution of onset latencies for PV neurons. $F = 1.579$, $P = 0.207$, ANOVA test. (*H*) Distribution of onset latencies for SOM neurons. (*I*) Distribution of onset latencies for VIP neurons. (*J*) Normalized amplitudes for different cell types. The adjusted amplitudes were normalized to the global average amplitude of L4 excitatory neuron responses. The black curve represents the laminar distribution of fluorescence intensity (in arbitrary unit) of thalamocortical axon fibers. (*K*) Average normalized peak amplitudes of different cell types in different layers. Arrows point to zero values. ***$P < 0.001$, *t*-test. (*L*) Percentage of cells exhibiting thalamocortical responses. Arrows point to zero values. L1 cell (12/ 22); Pyramidal cell (11/15 in L2/3; 18/18 in L4; 12/12 in L5; 8/10 in L6); PV cell (11/14 in L2/3;13/13 in L4; 15/15 in L5; 8/8 in L6); VIP cell (0/17 in L2/3; 6/16 in L4; 0/10 in L5; 0/6 in L6); SOM cell (1/12 in L2/3; 5/14 in L4; 0/10 in L5; 0/6 in L6).

Discussion

In this study, we intended to provide a comprehensive characterization of thalamocortical responses in different neuronal cell types across all cortical laminae, so as to generate a clear overall picture of thalamocortical innervation of the sensory cortex. By exploiting cell-type-specific transgenic mouse lines and taking an approach of ChR2-mediated axonal stimulation, a method that can activate known populations of axons even when severed from parent cell bodies (Petreanu et al. 2009; Cruikshank et al. 2010), we were able to achieve the specificity for examining monosynaptic thalamocortical inputs to desired target cells. To our knowledge, only one previous study (Cruikshank et al. 2010, in the barrel cortex) compared thalamocortical responses of PV, SOM and excitatory cells in both granular and infragranular layers. Inputs to L2/3 have not been examined, nor have L5 and L6 been distinguished. Our results for the first time revealed properties of thalamocortical innervation of different cell types across all layers in the auditory as well as visual cortex.

Consideration on the Limitations of the Current Method

In recent years, optogenetics has been widely applied in studies of neural circuits. Although it provides the specificity for

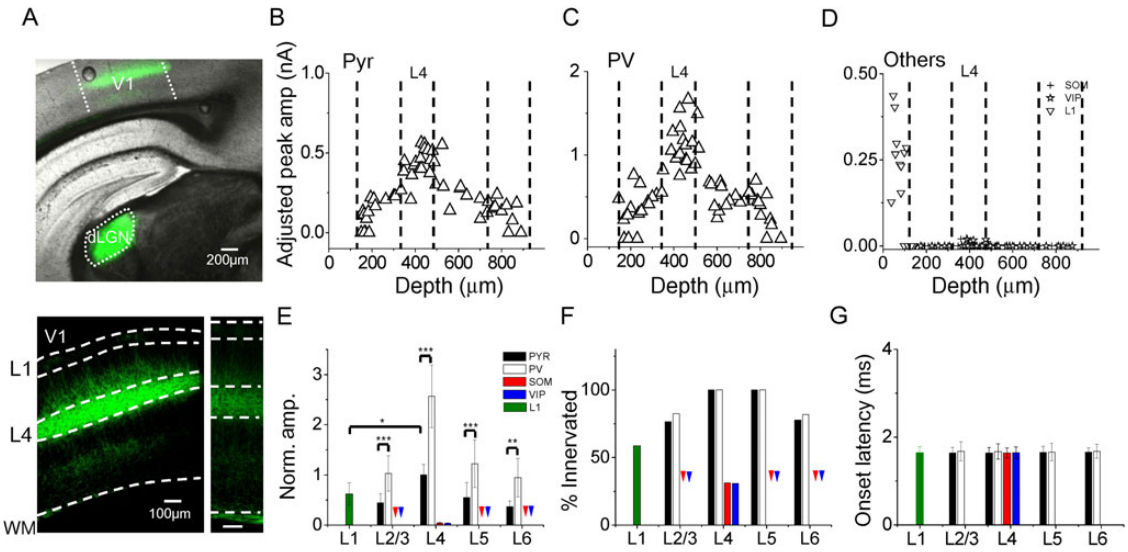

Figure 5. Laminar patterns of thalamocortical innervation of V1 neurons. (*A*) Top, superimposed fluorescence and bright field image of a brain slice showing ChR2 expression in the injected site (dLGN) and in the V1. Bottom, enlarged image of the V1 showing the fluorescent thalamic axons. Bottom right, image obtained with a lower level of exposure to show that there were no retrogradely labeled cell bodies. Scale: 100 μm. (*B*) Distribution of adjusted peak amplitudes for pyramidal neurons across cortical depth. $F = 34.553$, $P = 0.000$, ANOVA test. $P < 0.001$ between L4 and L2/3, $P < 0.001$ between L4 and L5, $P < 0.001$ between L4 and L6, post hoc test. (*C*) Distribution of adjusted response amplitudes for PV neurons. $F = 23.180$, $P = 0.000$, ANOVA test. $P < 0.001$ between L4 and L2/3, $P < 0.001$ between L4 and L5, $P < 0.001$ between L4 and L6, post hoc test. (*D*) Distribution of adjusted response amplitudes for other neuronal types. (*E*) Average normalized amplitudes for different cell types in different layers of V1. Arrows point to zero values. ***$P < 0.001$, **$P < 0.01$, *$P < 0.05$, *t*-test. (*F*) Percentage of cells exhibiting thalamocortical responses. Arrows point to zero values. L1 cell (10/17); Pyramidal cell (15/19 in L2/3; 19/19 in L4; 8/8 in L5; 7/9 in L6); PV cell (14/17 in L2/3; 15/15 in L4; 15/15 in L5; 9/11 in L6); SOM cell (0/12 in L2/3; 5/15 in L4; 0/7 in L5; 0/5 in L6); VIP cell (0/5 in L2/3; 4/9 in L4; 0/9 in L5; 0/5 in L6). (*G*) Average onset latencies for different cell types in different layers. $F = 0.112$, $P = 0.978$, ANOVA test.

Table 1 Summary of thalamocortical response properties for all cell types in the A1 and V1

Area	Cell type	Layer	Cell number	Adjusted amplitude[a] (pA)	Onset latency (ms)	Rise time (ms)	Duration (ms)	Half-peak duration (ms)
A1	L1	L1	22	425 ± 129	1.8 ± 0.2	9.0 ± 2.5	40.0 ± 11.2	16.1 ± 4.7
	Pyr	L2/3	15	129 ± 75	1.8 ± 0.3	14.6 ± 4.3	41.0 ± 9.7	23.6 ± 7.0
		L4	18	418 ± 180	1.7 ± 0.3	10.9 ± 5.3	31.3 ± 11.6	19.5 ± 7.9
		L5	12	195 ± 58	1.6 ± 0.3	14.8 ± 2.5	45.1 ± 8.0	27.8 ± 6.2
		L6	10	132 ± 70	1.5 ± 0.2	14.1 ± 3.3	43.1 ± 7.1	25.9 ± 4.1
	PV	L2/3	14	269 ± 168	1.7 ± 0.3	15.5 ± 2.6	43.3 ± 3.8	26.2 ± 3.7
		L4	13	962 ± 341	1.7 ± 0.4	14.7 ± 1.4	40.6 ± 6.5	24.9 ± 2.8
		L5	15	426 ± 130	1.7 ± 0.3	15.7 ± 1.8	42.8 ± 7.2	27.3 ± 5.4
		L6	8	426 ± 50	1.6 ± 0.4	15.8 ± 0.9	42.3 ± 4.4	26.8 ± 3.0
	SOM	L4	14	20 ± 7	1.6 ± 0.2	19.3 ± 5.6	30.8 ± 11.4	14.2 ± 6.2
	VIP	L4	16	24 ± 11	1.6 ± 0.2	28.6 ± 7.0	28.2 ± 6.6	16.8 ± 7.0
V1	L1	L1	17	271 ± 95	1.6 ± 0.1	11.9 ± 4.4	35.8 ± 6.0	22.8 ± 4.8
	Pyr	L2/3	19	190 ± 78	1.6 ± 0.1	13.9 ± 1.92	51.5 ± 12.8	28.6 ± 7.2
		L4	19	430 ± 97	1.7 ± 0.1	12.9 ± 1.0	48. ± 14.0	26.6 ± 8.4
		L5	8	190 ± 73	1.7 ± 0.1	13.9 ± 1.2	49.7 ± 10.0	33.7 ± 12.0
		L6	9	160 ± 49	1.7 ± 0.1	13.8 ± 1.2	49.7 ± 3.1	37.6 ± 5.0
	PV	L2/3	17	475 ± 178	1.7 ± 0.2	13.2 ± 0.7	47.1 ± 10.6	22.0 ± 6.3
		L4	15	1111 ± 260	1.7 ± 0.2	12.5 ± 0.7	41.4 ± 14.0	22.2 ± 4.3
		L5	15	596 ± 317	1.7 ± 0.2	13.8 ± 0.8	47.7 ± 9.2	24.1 ± 6.2
		L6	11	412 ± 167	1.7 ± 0.1	13.2 ± 1.1	48.4 ± 3.5	25.9 ± 1.1
	SOM	L4	15	18 ± 4.5	1.6 ± 0.1	21.9 ± 4.5	37.4 ± 7.8	18.3 ± 3.0
	VIP	L4	13	17 ± 2.0	1.7 ± 0.1	22.4 ± 2.2	37.2 ± 4.4	19.9 ± 3.4

Note: Data presented are mean ± SD.
[a]To quantify the adjusted amplitudes, cells which did not exhibit significant thalamocortical responses were excluded.

manipulating targeted neuronal projections better than electrical stimulation, some limitations of the method should not be overlooked.

Firstly, we should note that the optogenetic stimulation is different from the activation of thalamic axons by sensory input under physiological conditions. The optogenetic stimulation

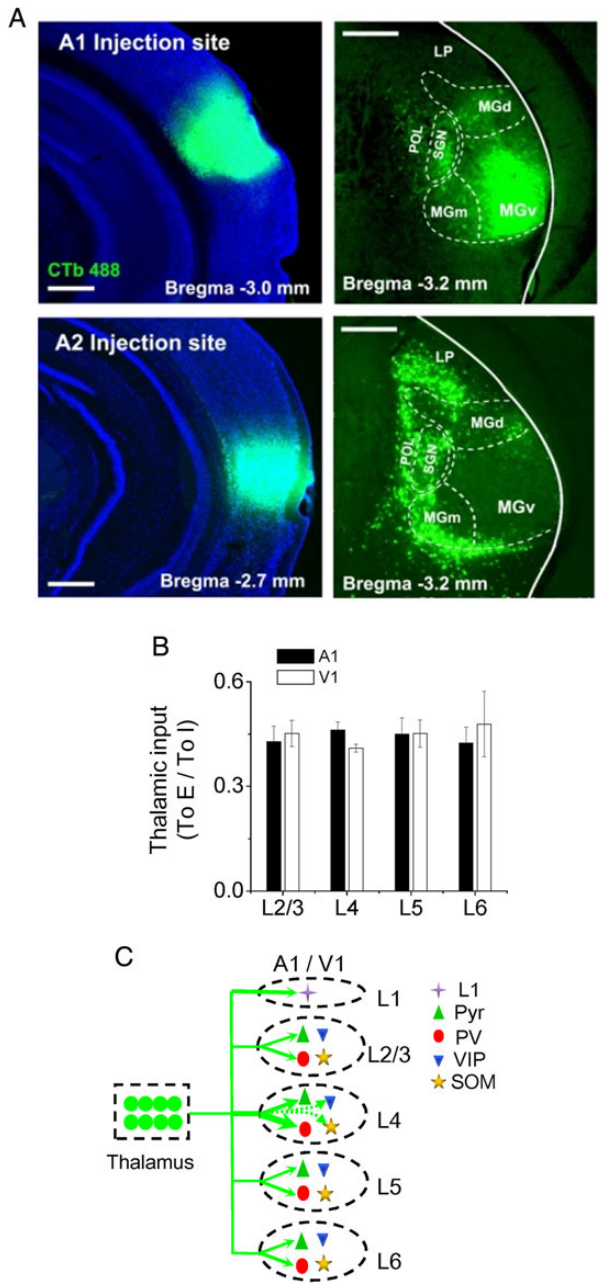

Figure 6. Summary of thalamocortical innervation of A1 and V1 neurons. (*A*) Top, image of CTb fluorescence in the injected site (in A1) (left) and retrogradely labeled neurons in the thalamus. Boundaries for some thalamic divisions are marked. Scale: 500 μm. LP: lateral posterior nucleus. SG: suprageniculate nucleus. POL: posterior limiting nucleus. MGd, MGm, MGv: dorsal, medial, and ventral part of the MGB respectively. (*B*) Ratio of strength of thalamocortical innervation of a pyramidal vs. a PV cell in the same layer. Average values were obtained by bootstrap sampling (1000 times, see Materials and Methods). Bar = SD. There are no significant differences between any 2 layers in either A1 or V1 (ANOVA test). (*C*) Schematic graph to summarize thalamocortical innervation patterns in the A1 and V1. The thickness of the green arrow indicates the innervation strength. Arrows with dashed lines represent the weakest connections.

will likely activate all the ChR2-expressing thalamocortical axons impinging on the recorded neuron, whereas in physiological conditions usually only a specific subset of thalamocortical inputs would be activated by a certain sensory stimulus. Our results cannot differentiate between situations where cortical neurons receive inputs from a wide range of thalamic neurons corresponding to a wide range of frequencies (in A1 for example), and where neurons receive inputs with very sharply tuned receptive fields, since the neurons with wider receptive fields would appear to receive a stronger input using our method, even though under normal physiological conditions they may be excited less than the more sharply tuned neurons. Thus, the current method only provides an estimation of total possible thalamic drive on a cortical neuron.

Secondly, it should be noted that the amplitude of the recorded response reflects a summation of all the anatomical synapses (boutons). In our experiments, a stronger response of one neuron compared with another could indicate that the neuron is receiving inputs from more presynaptic neurons due to higher convergence, that the neuron is receiving more boutons per presynaptic neuron, or that each bouton is releasing more neurotransmitter. These are 3 different mechanisms with different consequences for the cortical circuit. However, they cannot be differentiated using the current method.

Thirdly, previous studies suggest that projections from the core thalamic nucleus (the ventral part of the MGB, MGBv) and thalamic nuclei surrounding the MGBv may have different cortical area and layer preferences, with the latter particularly preferring layer 1 and infragranular zones (Ryugo and Killackey 1974; Frost and Caviness 1980; Herkenham 1980; Linke 1999; Linke and Schwegler 2000; Smith et al. 2010). Our post hoc examination of infected brains revealed that in most cases AAV infection covered multiple divisions of the MGB, raising the possibility that the recorded responses, in particular in layer 1 and infragranular zones, might have multiple input sources. In our retrograde tracing experiments, we found that the thalamic inputs to A1 are primarily from the MGBv, and that the inputs to A2 are almost exclusively from thalamic nuclei surrounding the MGBv (Fig. 6A). These observations are consistent with the anterograde tracing results published online by Allen Brain Atlas: mouse connectivity (connectivity.brain-map.org), in that MGBv projects strongly and almost exclusively to A1 (including its layer 1), and that MGBd and MGBm primarily project to regions dorsal and ventral to A1. Considering these anatomical results, we reason that the responses recorded in A1 neurons in our experiments largely reflect inputs from the MGBv. Nevertheless, we cannot exclude the possibility that thalamic nuclei other than the MGBv also contribute importantly to the responses in A1, with their inputs carrying information distinct from the MGBv. It will be an important topic to investigate in the future the respective thalamocortical projections from different thalamic nuclei with more focal viral injections.

Extensive Thalamic Innervation of Excitatory Neurons

It is generally thought that L4 (together with deep L3) is a major thalamorecipient layer (Romanski and LeDoux 1993; Huang and Winer 2000; Winer et al. 2005; Smith et al. 2012), and that L6 is another thalamorecipient layer in order to form a thalamo-cortico-thalamic loop (Sherman and Guillery 2002; Llano and Sherman 2008; Zhou et al. 2010). However, this view has long been challenged by in vivo and in vitro evidence suggesting that L2/3 and L5 also receive direct thalamic input (White 1978; Mitani et al. 1985; Agmon and Connors 1992; Romanski and LeDoux 1993; Citas et al. 1999; Viaene et al. 2011a; 2011b; Smith et al. 2012; Constantinople and Bruno 2013; Sun et al. 2013). In the present study, we systematically compared the laminar distribution of thalamocortical innervation strengths. For excitatory neurons, we confirmed that thalamic axons widely innervate them in all layers.

However, the thalamic drive to L4 cells is at least twice as strong as that to cells in other layers. This result supports the notion that L4 is the primary recipient layer for thalamically relayed sensory information, in particular from the core thalamic nucleus. The laminar pattern of the innervation strength correlates well with that of the density of thalamic axonal fibers, indicating that thalamic fiber density primarily determines the strength of innervation of a cortical layer.

The functional contribution of thalamocortical inputs to sensory processing in different cortical layers remains to be further investigated. In our previous in vivo studies in the A1, we have shown that thalamocortical inputs at least determine the onset latencies of sound-evoked excitatory synaptic responses as well as their overall responding frequency ranges in L4, L5, and L6 (Liu et al. 2007; Zhou et al. 2010; Li, Li et al. 2013; Sun et al. 2013). The lower probability of thalamic innervation of the upper part of L2/3 (Fig. 2*B*) is also consistent with our in vivo results showing that the excitatory inputs to upper L2/3 excitatory neurons have longer onset latencies than their L4 counterparts (Li, Ji, et al. 2014). It is possible that the extensive innervation of excitatory neurons allows the thalamically relayed information to be independently processed in different cortical layers in parallel. Another possibility is that a copy of thalamic information is input into layers other than L4, which provides a background reference as to prevent distortions of information during vertical processing in a cortical column.

A Matching Pattern of Thalamocortical Innervation of PV Neurons

Our results revealed that PV inhibitory neurons across layers (L2/3 to L6) are strongly innervated by thalamocortical axons. This finding well explains the in vivo results that tone-evoked spiking responses of fast-spiking or genetically identified PV neurons occur as early as or even earlier than their excitatory counterparts in supragranular, granular, and infragranular layers of the A1 (Wu et al. 2008; Zhou et al. 2010; Moore and Wehr 2013; Sun et al. 2013; Li, Xiong, et al. 2015). Interestingly, there is a great similarity in the innervation pattern between PV and excitatory neurons. Both receive strongest thalamic inputs in L4 as compared with other layers, and both are much more strongly driven by thalamic axons compared with other cell types in the same layer. The latter finding is also consistent with other in vitro results showing that fast-spiking (FS) and regular-spiking (RS) neurons display stronger responses to stimulation of thalamocortical axons as compared with other electrophysiologically identified cell types (Gibson et al. 1999; Beierlein et al. 2003; Cruikshank et al. 2010). These results thus strongly suggest that excitatory and PV cells are the major recipient neurons for ascending sensory inputs.

In each individual layer, the thalamocortical responses are substantially stronger in PV than excitatory cells. These overall differences in PV versus excitatory cell response amplitudes are in line with many in vitro reports on FS and RS cell responses using electrical or optogenetic stimulation (Gibson et al. 1999; Porter et al. 2001; Beierlein et al. 2003; Gabernet et al. 2005; Rose and Metherate 2005; Inoue and Imoto 2006; Sun et al. 2006; Cruikshank et al. 2007, 2010; Schiff and Reyes 2012; Kloc and Maffei 2014), as well as in vivo recording results for presumptive or genetically labeled PV and excitatory neurons (Simons and Carvell 1989; Swadlow 1989,1990; Ma et al. 2010; Li, Xiong, et al. 2015). The differential strengths are comparable with previous reports on unitary (i.e., single-axon) thalamocortical responses (Gabernet et al. 2005; Cruikshank et al. 2007), suggesting that the cell-type differences in the large synaptic currents recorded in our study may be accounted for at least partially by differences in unitary strengths.

Both slice recordings with electrical stimulation of thalamocortical axon tracts and in vivo intracellular recordings with sensory stimulation reveal that inhibitory input often follows excitatory input after a brief delay (Wehr and Zador 2003; Zhang et al. 2003; Gabernet et al. 2005; Wu et al. 2008; Li, Ji, et al. 2014). This phenomenon of feedforward inhibition appears predominant across cortical layers, with a possible exception of a subpopulation of principal neurons in L6 (Zhou et al. 2010). It has been shown to be important for regulating the timing of firing of pyramidal cells (Wehr and Zador 2003; Gabernet et al. 2005; Higley and Contreras 2006; Cruikshank et al. 2007; Zhou et al. 2012). Here we demonstrate that in each individual layer, PV neurons receive strong direct thalamic drive in parallel with pyramidal cells, distinct from SOM and VIP neurons. This finding is consistent with the notion that PV cells are the major presynaptic interneuron type that accounts for the sensory-evoked feedforward inhibition to pyramidal cells. The thalamic drive to PV cells is stronger than that to pyramidal cells, which ensures that PV cells can spike rapidly and reliably in response to ascending sensory inputs (Gabernet et al. 2005; Cruikshank et al. 2007; Ma et al. 2010; Moore and Wehr 2013; Li, Xiong, et al. 2015). Interestingly, the ratio between thalamic innervation strengths of PV and pyramidal cells is relatively constant across layers (Fig. 6*B*). This suggests that the strength of feedforward inhibition may be tightly regulated according to that of thalamic input to excitatory neurons, which can help to achieve the widely observed excitation-inhibition balance in cortical cells' responses to sensory stimulation (Wehr and Zador 2003; Zhang et al. 2003; Higley and Contreras 2006; Wu et al. 2008; Zhou et al. 2014).

Thalamocortical Innervation of Other Inhibitory Neurons

In contrast to the extensive thalamic innervation of PV neurons, SOM and VIP neurons barely receive direct thalamic inputs. In supra- and infragranular layers, SOM and VIP neurons are essentially not innervated by thalamic axons. In layer 4, only a subset of SOM and VIP neurons are innervated by thalamic axons, and the innervation is in general much weaker compared with excitatory and PV cells. The result on thalamocortical innervation of L4 VIP neurons is consistent with the anatomical findings of thalamocortical synaptic contacts on VIP neurons in the barrel and visual cortex (Staiger et al. 1996; Hajós et al. 1997). In addition, the finding of L4 SOM neurons responding weakly to activation of thalamic pathways is consistent with many previous results on physiologically identified low-threshold spiking cells, which likely correspond to SOM neurons (Gibson et al. 1999; Beierlein et al. 2003; Cruikshank et al. 2010; Takesian et al. 2013), or genetically labeled SOM cells (Tan et al. 2008; Cruikshank et al. 2010). Therefore, under single activation of thalamic pathways, SOM and VIP neurons are unlikely to contribute significantly to the feedforward inhibition (also see Li, Ji, et al. 2014), whereas they are better suited to provide pyramidal cells with feedback inhibition (Kapfer et al. 2007; Silberberg and Markram 2007; Berger et al. 2010; Ma et al. 2010; Adesnik et al. 2012; Xu et al. 2013). However, it has been shown that SOM neurons receive strongly facilitating excitatory inputs (Tan et al. 2008; Takesian et al. 2013), indicating that these cells can be activated by prolonged thalamocortical activation (Porter et al. 2001; Tan et al. 2008).

Interestingly, our data demonstrate that inhibitory cells in L1 receive relatively strong ascending thalamic inputs. This finding

is consistent with previous anatomical studies in auditory and visual cortices (Huang and Winer 2000; Cruz-Martín et al. 2014), and also with a recent functional study of matrix thalamic inputs to the prefrontal cortex (Cruikshank et al. 2012). Since L1 neurons are all inhibitory and can inhibit both excitatory and inhibitory cells in other layers (Jiang et al. 2013), it remains unclear what are the functional roles of the ascending inputs to L1 neurons in sensory processing. One possibility is that L1 may serve to mediate interactions between the nonlemniscal and lemniscal projection pathways (Cruikshank et al. 2002; Winer et al. 2005).

Taken together, the revealed laminar patterns of thalamocortical innervation in the sensory cortex of 2 different modalities highlight the necessity of considering parallel processing pathways (Fig. 6C) in addition to the conventional hierarchical processing pathway. Although the functional significance of thalamically relayed information in each individual lamina remains to be explored, the enriched laminar interactions/associations resulting from the extensive thalamocortical projections to all laminae may at least extend the computational power of sensory cortices.

Funding

This work was supported by National Institute of Health Grants DC008983 (to L.I.Z.) and EY019049 (to H.W.T.) and the David and Lucile Packard Foundation (Packard Fellowships for Science and Engineering) (to L.I.Z.). Z.X. and L.I.Z. were also supported by grants from the National Natural Science Foundation of China (U1301225, 31228013, 31171059) and a 973 program (2014CB943002) and Key Laboratory of Psychiatric Disorders of Guangdong Province.

Notes

We thank Leena A. Ibrahim for the help on confocal imaging. *Conflict of Interest*: None declared.

References

Adesnik H, Bruns W, Taniguchi H, Huang ZJ, Scanziani M. 2012. A neural circuit for spatial summation in visual cortex. Nature. 490:226–231.

Agmon A, Connors BW. 1992. Correlation between intrinsic firing patterns and thalamocortical synaptic responses of neurons in mouse barrel cortex. J Neurosci. 12:319–329.

Agmon A, Connors BW. 1991. Thalamocortical responses of mice somatosensory (barrel) cortex in vitro. Neuroscience. 41:365–379.

Armstrong-James M, Fox K, Das-Gupta A. 1992. Flow of excitation within rat barrel cortex on striking a single vibrissa. J Neurophysiol. 68:1345–1358.

Barkat TR, Polley DB, Hensch TK. 2011. A critical period for auditory thalamocortical connectivity. Nat Neurosci. 14:1189–1194.

Beierlein M, Gibson JR, Connors BW. 2003. Two dynamically distinct inhibitory networks in layer 4 of the neocortex. J Neurophysiol. 90:2987–3000.

Berger TK, Silberberg G, Perin R, Markram H. 2010. Brief bursts self-inhibit and correlate the pyramidal network. PLoS Biol. 8:e1000473.

Boyden ES, Zhang F, Bamberg E, Nagel G, Deisseroth K. 2005. Millisecond-timescale, genetically targeted optical control of neural activity. Nat Neurosci. 8:1263–1268.

Callaway EM. 1998. Local circuits in primary visual cortex of the macaque monkey. Annu Rev Neurosci. 21:47–74.

Cardin JA, Carlen M, Meletis K, Knoblich U, Zhang F, Deisseroth K, Tsai LH, Moore CI. 2009. Driving fast-spiking cells induces gamma rhythm and controls sensory responses. Nature. 459:663–667.

Chung S, Ferster D. 1998. Strength and orientation tuning of the thalamic input to simple cells revealed by electrically evoked cortical suppression. Neuron. 20:1177–1189.

Citas JS, de Venecia RK, McMullen NT. 1999. Thalamocortical afferents of Lorente de Nó: medial geniculate axons that project to primary auditory cortex have collateral branches to layer I. Brain Res. 830:203–208.

Constantinople CM, Bruno RM. 2013. Deep cortical layers are activated directly by thalamus. Science. 340:1591–1594.

Cruikshank SJ, Ahmed OJ, Stevens TR, Patrick SL, Gonzalez AN, Elmaleh M, Connors BW. 2012. Thalamic control of layer 1 circuits in prefrontal cortex. J Neurosci. 32:17813–17823.

Cruikshank SJ, Lewis TJ, Connors BW. 2007. Synaptic basis for intense thalamocortical activation of feedforward inhibitory cells in neocortex. Nat Neurosci. 10:462–468.

Cruikshank SJ, Rose HJ, Metherate R. 2002. Auditory thalamocortical synaptic transmission in vitro. J Neurophysiol. 87:361–384.

Cruikshank SJ, Urabe H, Nurmikko AV, Connors BW. 2010. Pathway-specific feedforward circuits between thalamus and neocortex revealed by selective optical stimulation of axons. Neuron. 65:230–245.

Cruz-Martín A, El-Danaf RN, Osakada F, Sriram B, Dhande OS, Nguyen PL, Callaway EM, Ghosh A, Huberman AD. 2014. A dedicated circuit links direction-selective retinal ganglion cells to the primary visual cortex. Nature. 507:358–361.

Douglas RJ, Martin KA. 2004. Neuronal circuits of the neocortex. Annu Rev Neurosci. 27:419–451.

Feldmeyer D. 2012. Excitatory neuronal connectivity in the barrel cortex. Front Neuroanat. 6:24.

Ferster D, Lindström S. 1983. An intracellular analysis of geniculocortical connectivity in area 17 of the cat. J Physiol. 342:181–215.

Frost DO, Caviness VS Jr. 1980. Radial organization of thalamic projections to the neocortex in the mouse. J Comp Neurol. 194:369–393.

Gabernet L, Jadhav SP, Feldman DE, Carandini M, Scanziani M. 2005. Somatosensory integration controlled by dynamic thalamocortical feed-forward inhibition. Neuron. 48:315–327.

Gibson JR, Beierlein M, Connors BW. 1999. Two networks of electrically coupled inhibitory neurons in neocortex. Nature. 402:75–79.

Gilbert CD, Wiesel TN. 1979. Morphology and intracortical projections of functionally characterized neurones in the cat visual cortex. Nature. 280:120–125.

Gradinaru V, Mogri M, Thompson KR, Henderson JM, Deisseroth K. 2009. Optical deconstruction of parkinsonian neural circuitry. Science. 324:354–359.

Hajós F, Staiger JF, Halasy K, Freund TF, Zilles K. 1997. Geniculocortical afferents form synaptic contacts with vasoactive intestinal polypeptide (VIP) immunoreactive neurons of the rat visual cortex. Neurosci Lett. 228:179–182.

Herkenham M. 1980. Laminar organization of thalamic projections to the rat neocortex. Science. 207:532–535.

Higley MJ, Contreras D. 2006. Balanced excitation and inhibition determine spike timing during frequency adaptation. J Neurosci. 26:448–457.

Huang CL, Winer JA. 2000. Auditory thalamocortical projections in the cat: laminar and areal patterns of input. J Comp Neurol. 427:302–331.

Inoue T, Imoto K. 2006. Feedforward inhibitory connections from multiple thalamic cells to multiple regular-spiking cells in

layer 4 of the somatosensory cortex. J Neurophysiol. 96:1746–1754.
Jiang X, Wang G, Lee AJ, Stornetta RL, Zhu JJ. 2013. The organization of two new cortical interneuronal circuits. Nat Neurosci. 16:210–218.
Kapfer C, Glickfeld LL, Atallah BV, Scanziani M. 2007. Supralinear increase of recurrent inhibition during sparse activity in the somatosensory cortex. Nat Neurosci. 10:743–753.
Kloc M, Maffei A. 2014. Target-specific properties of thalamocortical synapses onto layer 4 of mouse primary visual cortex. J Neurosci. 34:15455–15465.
Li LY, Ji XY, Liang F, Li YT, Xiao Z, Tao HW, Zhang LI. 2014. A feedforward inhibitory circuit mediates lateral refinement of sensory representation in upper layer 2/3 of mouse primary auditory cortex. J Neurosci. 34:13670–13683.
Li LY, Li YT, Zhou M, Tao HW, Zhang LI. 2013. Intracortical multiplication of thalamocortical signals in mouse auditory cortex. Nat Neurosci. 16:1179–1181.
Li LY, Xiong XR, Ibrahim LA, Yuan W, Tao HW, Zhang LI. 2015. Differential receptive field properties of parvalbumin and somatostatin inhibitory neurons in mouse auditory cortex. Cereb Cortex. 25:1782–1791.
Li YT, Ibrahim LA, Liu BH, Zhang LI, Tao HW. 2013. Linear transformation of thalamocortical input by intracortical excitation. Nat Neurosci. 16:1324–1330.
Lien AD, Scanziani M. 2013. Tuned thalamic excitation is amplified by visual cortical circuits. Nat Neurosci. 16:1315–1323.
Linke R. 1999. Organization of projections to temporal cortex originating in the thalamic posterior intralaminar nucleus of the rat. Exp Brain Res. 127:314–320.
Linke R, Schwegler H. 2000. Convergent and complementary projections of the caudal paralaminar thalamic nuclei to rat temporal and insular cortex. Cereb Cortex. 10:753–771.
Liu BH, Wu GK, Arbuckle R, Tao HW, Zhang LI. 2007. Defining cortical frequency tuning with recurrent excitatory circuitry. Nat Neurosci. 10:1594–1600.
Llano DA, Sherman SM. 2008. Evidence for nonreciprocal organization of the mouse auditory thalamocortical-corticothalamic projection systems. J Comp Neurol. 507:1209–1227.
Ma WP, Liu BH, Li YT, Huang ZJ, Zhang LI, Tao HW. 2010. Visual representations by cortical somatostatin inhibitory neurons—selective but with weak and delayed responses. J Neurosci. 30:14371–14379.
Madisen L, Mao T, Koch H, Zhuo JM, Berenyi A, Fujisawa S, Hsu YW, Garcia AJ 3rd, Gu X, Zanella S, et al. 2012. A toolbox of Cre-dependent optogenetic transgenic mice for light-induced activation and silencing. Nat Neurosci. 15:793–802.
Markram H, Toledo-Rodriguez M, Wang Y, Gupta A, Silberberg G, Wu C. 2004. Interneurons of the neocortical inhibitory system. Nat Rev Neurosci. 5:793–807.
Mitani A, Shimokouchi M, Itoh K, Nomura S, Kudo M, Mizuno N. 1985. Morphology and laminar organization of electrophysiologically identified neurons in the primary auditory cortex in the cat. J Comp Neurol. 235:430–447.
Moore AK, Wehr M. 2013. Parvalbumin-expressing inhibitory interneurons in auditory cortex are well-tuned for frequency. J Neurosci. 33:13713–13723.
Moore CI, Nelson SB. 1998. Spatio-temporal subthreshold receptive fields in the vibrissa representation of rat primary somatosensory cortex. J Neurophysiol. 80:2882–2892.
Nagel G, Szellas T, Huhn W, Kateriya S, Adeishvili N, Berthold P, Ollig D, Hegemann P, Bamberg E. 2003. Channelrhodopsin-2, a directly light-gated cation-selective membrane channel. Proc Natl Acad Sci USA. 100:13940–13945.
Oberlaender M, Ramirez A, Bruno RM. 2012. Sensory experience restructures thalamocortical axons during adulthood. Neuron. 74:648–655.
Petreanu L, Huber D, Sobczyk A, Svoboda K. 2007. Channelrhodopsin-2-assisted circuit mapping of long-range callosal projections. Nat Neurosci. 10:663–668.
Petreanu L, Mao T, Sternson SM, Svoboda K. 2009. The subcellular organization of neocortical excitatory connections. Nature. 457:1142–1145.
Pfeffer CK, Xue M, He M, Huang ZJ, Scanziani M. 2013. Inhibition of inhibition in visual cortex: the logic of connections between molecularly distinct interneurons. Nat Neurosci. 16:1068–1076.
Porter JT, Johnson CK, Agmon A. 2001. Diverse types of interneurons generate thalamus-evoked feedforward inhibition in the mouse barrel cortex. J Neurosci. 21:2699–2710.
Richardson RJ, Blundon JA, Bayazitov IT, Zakharenko SS. 2009. Connectivity patterns revealed by mapping of active inputs on dendrites of thalamorecipient neurons in the auditory cortex. J Neurosci. 29:6406–6417.
Romanski LM, LeDoux JE. 1993. Organization of rodent auditory cortex: anterograde transport of PHA-L from MGv to temporal neocortex. Cereb Cortex. 3:499–514.
Rose HJ, Metherate R. 2005. Auditory thalamocortical transmission is reliable and temporally precise. J Neurophysiol. 94:2019–2030.
Rudy B, Fishell G, Lee S, Hjerling-Leffler J. 2011. Three groups of interneurons account for nearly 100% of neocortical GABAergic neurons. Dev Neurobiol. 71:45–61.
Ryugo DK, Killackey HP. 1974. Differential telencephalic projections of the medial and ventral divisions of the medial geniculate body of the rat. Brain Res. 82:173–177.
Schiff ML, Reyes AD. 2012. Characterization of thalamocortical responses of regular-spiking and fast-spiking neurons of the mouse auditory cortex in vitro and in silico. J Neurophysiol. 107:1476–1488.
Sherman SM, Guillery RW. 2002. The role of the thalamus in the flow of information to the cortex. Philos Trans R Soc Lond B Biol Sci. 357:1695–1708.
Silberberg G, Markram H. 2007. Disynaptic inhibition between neocortical pyramidal cells mediated by Martinotti cells. Neuron. 53:735–746.
Simons DJ, Carvell GE. 1989. Thalamocortical response transformation in the rat vibrissa/barrel system. J Neurophysiol. 61:311–330.
Smith PH, Manning KA, Uhlrich DJ. 2010. Evaluation of inputs to rat primary auditory cortex from the suprageniculate nucleus and extrastriate visual cortex. J Comp Neurol. 518:3679–3700.
Smith PH, Uhlrich DJ, Manning KA, Banks MI. 2012. Thalamocortical projections to rat auditory cortex from the ventral and dorsal divisions of the medial geniculate nucleus. J Comp Neurol. 520:34–51.
Staiger JF, Zilles K, Freund TF. 1996. Innervation of VIP-immunoreactive neurons by the ventroposteromedial thalamic nucleus in the barrel cortex of the rat. J Comp Neurol. 367:194–204.
Sun QQ, Huguenard JR, Prince DA. 2006. Barrel cortex microcircuits: thalamocortical feedforward inhibition in spiny stellate cells is mediated by a small number of fast-spiking interneurons. J Neurosci. 26:1219–1230.
Sun YJ, Kim YJ, Ibrahim LA, Tao HW, Zhang LI. 2013. Synaptic mechanisms underlying functional dichotomy between intrinsic-bursting and regular-spiking neurons in auditory cortical layer 5. J Neurosci. 33:5326–5339.
Swadlow HA. 1990. Efferent neurons and suspected interneurons in S-1 forelimb representation of the awake rabbit: receptive fields and axonal properties. J Neurophysiol. 63:1477–1498.

Swadlow HA. 1989. Efferent neurons and suspected interneurons in S-1 vibrissa cortex of the awake rabbit: receptive fields and axonal properties. J Neurophysiol. 62:288–308.

Takesian AE, Kotak VC, Sharma N, Sanes DH. 2013. Hearing loss differentially affects thalamic drive to two cortical interneuron subtypes. J Neurophysiol. 110:999–1008.

Tamamaki N, Yanagawa Y, Tomioka R, Miyazaki J, Obata K, Kaneko T. 2003. Green fluorescent protein expression and colocalization with calretinin, parvalbumin, and somatostatin in the GAD67-GFP knock-in mouse. J Comp Neurol. 467:60–479.

Tan Z, Hu H, Huang ZJ, Agmon A. 2008. Robust but delayed thalamocortical activation of dendritic-targeting inhibitory interneurons. Proc Natl Acad Sci USA. 105:2187–2192.

Taniguchi H, He M, Wu P, Kim S, Paik R, Sugino K, Kvitsiani D, Fu Y, Lu J, Lin Y, et al. 2011. A resource of Cre driver lines for genetic targeting of GABAergic neurons in cerebral cortex. Neuron. 71:995–1013.

Viaene AN, Petrof I, Sherman SM. 2011a. Synaptic properties of thalamic input to layers 2/3 and 4 of primary somatosensory and auditory cortices. J Neurophysiol. 105:279–292.

Viaene AN, Petrof I, Sherman SM. 2011b. Synaptic properties of thalamic input to the subgranular layers of primary somatosensory and auditory cortices in the mouse. J Neurosci. 31:12738–12747.

Wang Y, Toledo-Rodriguez M, Gupta A, Wu C, Silberberg G, Luo J, Markram H. 2004. Anatomical, physiological and molecular properties of Martinotti cells in the somatosensory cortex of the juvenile rat. J Physiol. 561:65–90.

Wehr M, Zador AM. 2003. Balanced inhibition underlies tuning and sharpens spike timing in auditory cortex. Nature. 426:442–446.

White EL. 1978. Identified neurons in mouse Sml cortex which are postsynaptic to thalamocortical axon terminals: a combined Golgi-electron microscopic and degeneration study. J Comp Neurol. 181:627–661.

Winer JA, Miller LM, Lee CC, Schreiner CE. 2005. Auditory thalamocortical transformation: structure and function. Trends Neurosci. 28:255–263.

Wu GK, Arbuckle R, Liu BH, Tao HW, Zhang LI. 2008. Lateral sharpening of cortical frequency tuning by approximately balanced inhibition. Neuron. 58:132–143.

Xu H, Jeong HY, Tremblay R, Rudy B. 2013. Neocortical somatostatin-expressing GABAergic interneurons disinhibit the thalamorecipient layer 4. Neuron. 77:155–167.

Yamamoto T, Samejima A, Oka H. 1990. The mode of synaptic activation of pyramidal neurons in the cat primary somatosensory cortex: an intracellular HRP study. Exp Brain Res. 80:12–22.

Zhang LI, Tan AY, Schreiner CE, Merzenich MM. 2003. Topography and synaptic shaping of direction selectivity in primary auditory cortex. Nature. 424:201–205.

Zhou M, Liang F, Xiong XR, Li L, Li H, Xiao Z, Tao HW, Zhang LI. 2014. Scaling down of balanced excitation and inhibition by active behavioral states in auditory cortex. Nat Neurosci. 17:841–850.

Zhou Y, Liu BH, Wu GK, Kim YJ, Xiao Z, Tao HW, Zhang LI. 2010. Preceding inhibition silences layer 6 neurons in auditory cortex. Neuron. 65:706–717.

Zhou Y, Mesik L, Sun YJ, Liang F, Xiao Z, Tao HW, Zhang LI. 2012. Generation of spike latency tuning by thalamocortical circuits in auditory cortex. J Neurosci. 32:9969–9980.

Zingg B, Hintiryan H, Gou L, Song MY, Bay M, Bienkowski MS, Foster NN, Yamashita S, Bowman I, Toga AW, et al. 2014. Neural networks of the mouse neocortex. Cell. 156:1096–1111.